ELSEVIER

Available online at www.sciencedirect.com

SCIENCE DIRECT®

Microelectronic Engineering 80 (2005) 114–121

MICROELECTRONIC ENGINEERING

www.elsevier.com/locate/mee

Negative Bias Temperature Instability in CMOS Devices

S. Mahapatra, M. A. Alam*, P. Bharath Kumar, T. R. Dalei, D. Varghese and D. Saha

Department of Electrical Engineering, Indian Institute of Technology Bombay, Mumbai, India
**School of Electrical Engineering and Computer Science, Purdue University, West Lafayette, IN, USA*
Tel: 91-22-25720408 email: souvik@ee.iitb.ac.in

Abstract

This paper reviews the experimental and modeling efforts to understand the mechanism of Negative Bias Temperature Instability (NBTI) in p-MOSFETs, which is becoming a serious reliability concern for analog and digital CMOS circuits. Conditions for interface and bulk trap generation and their dependence on stress voltage and oxide field, temperature and time are discussed. The role of inversion layer holes, hot-holes and hot-electrons are also discussed. The recovery of generated damage and its bias, temperature and AC frequency dependence are discussed. The degradation and recovery is modeled using the standard Reaction-Diffusion theory, and some unique data scaling features are pointed out. The impact of gate-oxide nitridation is also reviewed.

Keywords: MOSFET; NBTI; interface traps; bulk traps; parameter instability; Reaction-Diffusion model; hydrogen diffusion

1. Introduction

Negative Bias Temperature Instability (NBTI) of p-MOSFET parameters (threshold voltage, linear and saturation drain current, gate-drain capacitance, etc.) is becoming a serious reliability concern for digital and analog CMOS circuits (see [1] and references therein). After extensive characterization it has been found [1-7] that NBTI (i) shows a t^n power law time dependence with n~0.17-0.3, (ii) is a temperature activated process with an activation energy (E_A) of 0.1-0.2eV, (iii) is more dominant for p-MOSFETs under inversion, (iv) anneals if stress is removed, (v) is reduced if deuterium anneal is used for passivation in place of hydrogen, (vi) is influenced by the presence of water, boron, and nitrogen in the gate oxide, and (vii) is due to either (or both) interface (N_{IT}) and bulk-trap (N_{OT}) generation.

There have been some efforts to model NBTI as well [8-10]. However, the basic NBTI mechanism is not yet fully understood. Moreover, NBTI has not been carefully studied for p-MOSFETs under non-zero substrate bias (V_B). This is an important concern since many circuits utilize V_B to control the device threshold voltage (V_T), (*e.g.*, for multiple V_T CMOS, standby leakage reduction, etc.). As of today, the issues of interest are: (i) generation of N_{IT} and N_{OT}

0167-9317/$ - see front matter © 2005 Published by Elsevier B.V.
doi:10.1016/j.mee.2005.04.053

and their gate bias (V_G), V_B, temperature (T), and time (t) dependence; (ii) recovery of N_{IT} and N_{OT} and their V_G, T and AC frequency (f) dependence, and (iii) impact of nitrogen on N_{IT} and N_{OT}. Proper understanding of the complete NBTI mechanism will help determine (i) reliability budget for a technology node, (ii) burn-in and test conditions, (iii) TCAD and SPICE models, and (iv) process parameters for NBTI control. This paper attempts to develop a consistent picture of the NBTI phenomenon under a wide range of operating conditions, and identifies possible areas where the present understanding is incomplete and requires further attention.

2. Proper choice of stress gate bias

Fig.1 shows the time evolution of ΔV_T and SILC for T_{PHY}=36Å devices under different stress V_G. For low stress V_G, ΔV_T shows the well-known power law in time with exponent 0.25. For high stress V_G, ΔV_T increases at longer time and shows much larger time exponent. SILC is not seen for low stress V_G but is observed for high stress V_G. The onset (in time) and magnitude of SILC coincides with that of enhanced ΔV_T at high stress V_G. It is obvious that such long-time ΔV_T increase at high stress V_G seriously affects extrapolated lifetime and related voltage acceleration analysis, and hence calls for careful attention.

Fig.2 shows p-MOSFET energy band diagram in inversion at low and high V_G. At low V_G, electrons tunnel from gate and holes tunnel from substrate. At high V_G, electrons tunnel from gate and cause impact ionization at the substrate and thereby generate hot holes (HH). These generated HH inject back into the oxide and is responsible for N_{OT} generation [4,11].

Note that in general, ΔV_T is due to both ΔN_{IT} and ΔN_{OT}. Since the appearance of SILC indicates ΔN_{OT} (as SILC monitors mid-oxide traps) [11], it is clear that long-time enhanced ΔV_T at high stress V_G is due to (hole trapping in) ΔN_{OT} [4]. This is verified by the calculated ΔN_{OT} contributions (shown by the lines in Fig.1). As ΔN_{OT} is a strongly V_G activated process, it becomes negligible compared to ΔN_{IT} at lower stress V_G. Therefore, NBTI must always be evaluated at low to moderate V_G to avoid impact ionization, HH generation and undesirable contribution from ΔN_{OT}.

As a proof, Fig.3 plots ΔV_T versus ΔN_{IT} for a wide range of stress V_G. The maximum V_G was kept low to avoid HH generation in this device. Excellent correlation over a wide range of V_G suggests the absence of ΔN_{OT}. Otherwise, strong V_G acceleration of ΔN_{OT} would result in higher ΔV_T for a given ΔN_{IT} with increasing V_G. Therefore, NBTI is only due to interface trap generation for lower (proper) stress V_G.

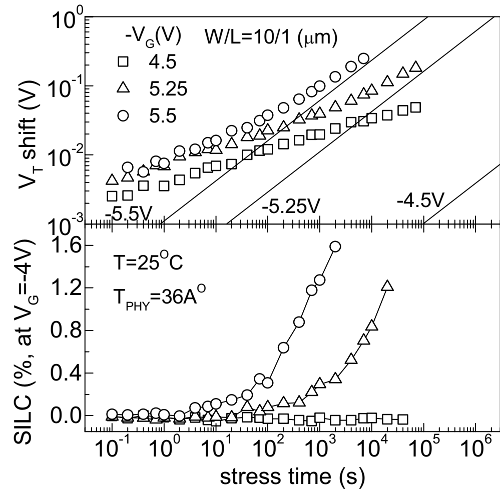

Fig. 1. (Top) Time evolution of V_T shift for stress at various V_G (symbols). Calculated ΔN_{OT} contributions are shown as lines. (Bottom) Time evolution of Stress Induced Leakage Current (SILC) for various stress V_G. Devices with thermal (non-nitrided) gate oxides. Data from [4].

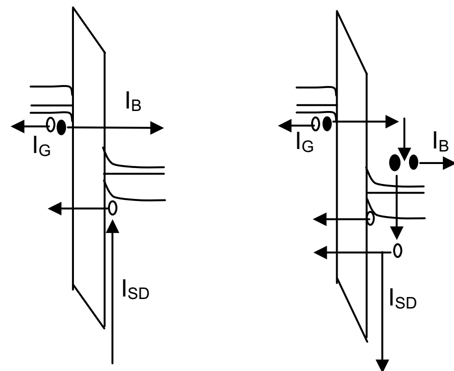

Fig. 2. p-MOSFET energy band diagram in inversion under low (LHS) and high (RHS) V_G. Electron (solid circle) and hole (open circle) currents are shown.

As a guideline for choosing maximum stress V_G, Fig.4 shows measured gate (I_G), substrate (I_B) and source/drain (I_{SD}) current as a function of V_G using carrier separation measurement. According to Fig.2, $I_G=I_B+I_{SD}$ for low stress V_G, where I_B and I_{SD} are respectively due to electrons and holes tunneling

from gate to substrate and source/drain to gate. For high stress V_G, $I_B = I_G + I_{SD}$ and the holes generated out of impact ionization flow out of source/drain and cause a sign reversal for I_{SD}. The "dip" in I_{SD} (V_G) characteristics indicates significant presence of HH. V_G for NBTI stress must be chosen below this point to ensure negligible ΔN_{OT} and $\Delta V_T \sim \Delta N_{IT}$ only.

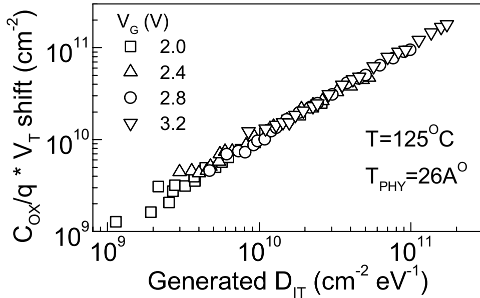

Fig. 3. Correlation of ΔV_T and ΔD_{IT} for a wide stress V_G range on devices having thermal, non-nitrided oxide. Maximum V_G kept low to avoid impact ionization. ΔD_{IT} ($=\Delta N_{IT}/\Delta E$) obtained from charge pumping, ΔE (energy zone of recombination) determined in pre-stress from multi-frequency measurements. Data from [5].

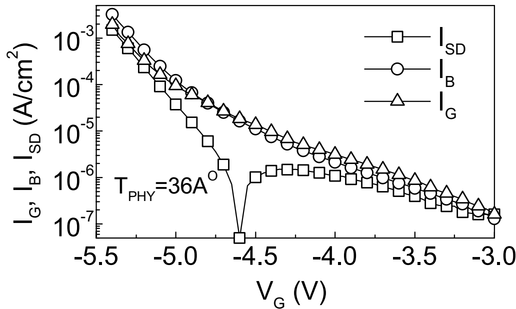

Fig. 4. Gate, substrate and source/drain current as a function of V_G from carrier separation measurements under V_B=0V.

3. Factors influencing interface-trap generation

Fig. 5 shows correlation of ΔV_T (under properly chosen stress condition such that $\Delta V_T \sim \Delta N_{IT}$) versus stress oxide field (E_{OX}) and stress V_G for different T_{PHY} devices. Note that ΔN_{IT} is governed by E_{OX} and not V_G. As a further proof, Fig. 6 plots normalized (to initial value) ΔI_D (measured under a constant gate overdrive, represents mobility degradation ~ ΔN_{IT}) as a function of time for p-MOSFET inversion (PINV) and n-MOSFET accumulation (NACC) stress. Due to difference in flatband voltage, $V_G|_{NACC} = V_G|_{PINV} - 1$ for having identical E_{OX}. It can be clearly seen that the degradation is identical when compared under identical E_{OX} (and not under identical V_G).

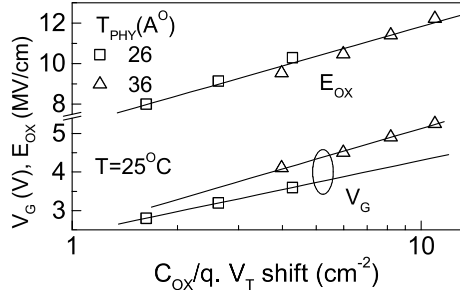

Fig. 5. Correlation of ΔV_T (~ ΔN_{IT}) against V_G (Y axis, lower part) and E_{OX} (Y axis, upper part) during 1000s stress for different T_{PHY} devices (thermal, non-nitrided oxide). Data from [5].

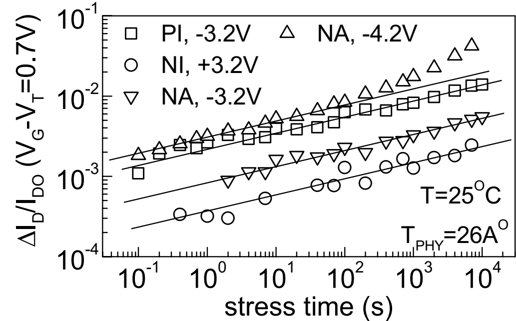

Fig. 6. Time evolution of normalized I_D degradation for n- and p-MOSFETs (thermal, non-nitrided oxide) under different stress configurations. Data from [5].

Fig. 6 also shows normalized ΔI_D for n-MOSFET inversion (NINV) stress under identical E_{OX} as PINV stress. PINV shows much larger ΔN_{IT} than NINV, indicating possible role of holes. Note, availability of holes at the Si/SiO_2 interface is more for PINV stress (inversion layer) compared to NINV stress (tunneling from gate). The role of holes is further verified in Fig. 7, which shows ΔV_T as a function of inversion hole density for different T_{PHY}. Excellent correlation over a wide range of T_{PHY} again indicates that holes play an important role behind N_{IT} generation.

Fig. 8 plots ΔV_T versus energy dissipated by hot electrons (tunneling from gate) at Si/SiO_2 interface for different T_{PHY} devices. The absence of correlation clearly shows that hot electrons do not play a role behind ΔN_{IT}. Note that the absence of ΔV_T versus V_G correlation (Fig. 5) also suggests that hot electrons do not play a role behind ΔN_{IT} even when their energy is

considered in the ballistic limit (E ~ q. V_G). All the above results clearly show that ΔN_{IT} during NBTI stress is governed by E_{OX} and inversion holes.

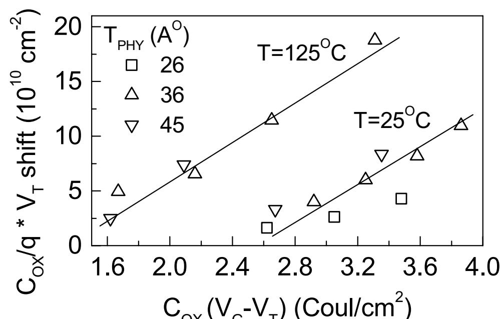

Fig. 7. Correlation of ΔV_T (~ΔN_{IT}) versus inversion hole density for different T_{PHY} devices (thermal, non-nitrided oxide). Data from [4].

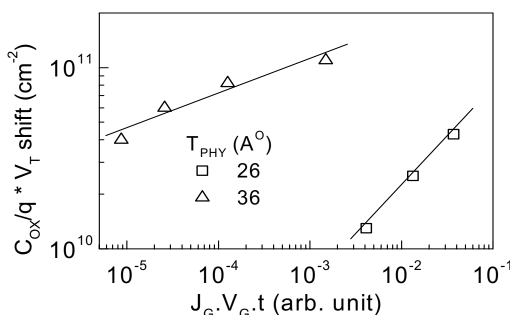

Fig. 8. ΔV_T (~ΔN_{IT}) as a function of energy dissipated by electrons tunneling from gate for different T_{PHY} devices (thermal, non-nitrided oxide). Data from [4].

4. Model for interface-trap generation

N_{IT} generation during NBTI has been explained using the Reaction-Diffusion (R-D) model [8]. The model states that ΔN_{IT} is due to the dissociation of Si-H bonds at the Si/SiO_2 interface (reaction) and the subsequent movement of released H species away from the interface (diffusion) which leaves behind Si- (N_{IT}). The model in its basic form does not say how the reaction takes place, or for that matter what is the nature (neutral/charged) of the diffusing species.

Though the exact reaction process is unknown, it is speculated that inversion layer holes tunnel into the oxide and are captured by Si-H bonds. This makes the Si-H bonds weak, which are subsequently broken by thermal excitation or otherwise. Several reaction pathways are possible (h = holes, H^+ = ionic, H^0 = atomic and H_2 = molecular hydrogen) [10]:

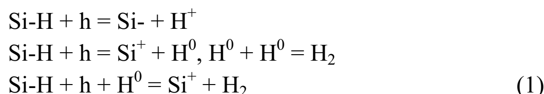

$$\text{Si-H} + h = \text{Si-} + H^+$$
$$\text{Si-H} + h = Si^+ + H^0,\ H^0 + H^0 = H_2$$
$$\text{Si-H} + h + H^0 = Si^+ + H_2 \quad (1)$$

Time evolution of ΔN_{IT} is governed by the following coupled differential equations [8-10]:

$$dN_{IT}/dt = k_F\,[N_0 - N_{IT}] - k_R\,N_H(x=0)\,N_{IT}$$
$$dN_H/dt = D\,d^2N_H/dx^2 \quad (2)$$

where k_F, k_R are the forward and reverse reaction rates, N_0 is the total density of Si-H bonds, N_H and D respectively are the concentration and diffusivity of released H species. The R-D model and its solution are explained in Fig. 9.

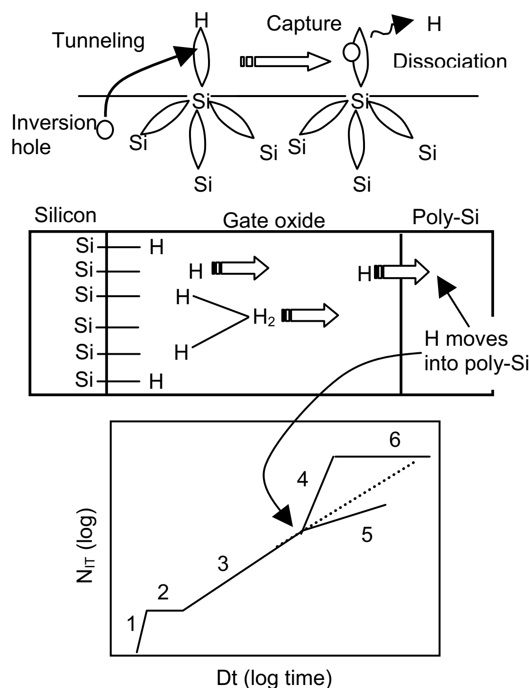

Fig. 9. R-D model showing the hole induced rupture of Si-H bonds and subsequent diffusion of H species. The model's solution shows various phases of N_{IT} buildup. (1) reaction limited, (2) quasi-equilibrium, before the onset of H diffusion, (3) diffusion in the oxide till H diffusion front hits poly-Si, (4) faster degradation due to H absorption into poly-Si after H diffusion front hits poly-Si (absorbing poly-Si), (5) saturation due to H reflection from poly-Si after H diffusion front hits poly-Si (reflecting poly-Si), (6) saturation due to all Si-H broken. [7,9].

Though the general solution of R-D model shows different phases (see Fig.9), for typical measurement

condition phase-3 (and beyond) are experimentally observed. Recently, the coupled R-D equations have been numerically solved [9,10]. It has been shown that the power law time exponent in phase-3 depends on the nature of the diffusing species [10], as listed in Table-I. Typical H diffusion profile as obtained using numerical simulation (for H^0) is shown in Fig. 10.

Species	Exponent
H^0	0.25
H_2	0.165
H^0, H_2	0.165 – 0.25
H^+	0.5
H^0, H_2, H+	0.165 – 0.5
Trap or Release	Increase or decrease

Table-I. Simulated power law time exponent in phase-3 for different diffusing species [10].

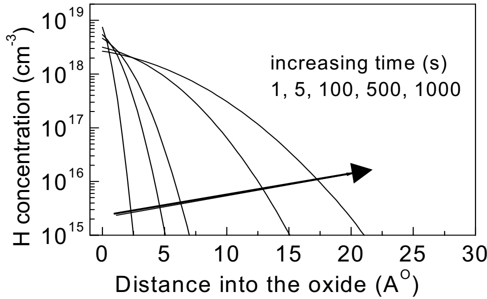

Fig. 10. H profile during NBTI stress (phase-3). Peak H concentration reduces while its spread broadens with time. $K_F=10^{-2}/s$, $k_R=10^{-18}cm^3/s$, $N_0=10^{14}/cm^2$, $D=10^{-17}cm^2/s$.

5. Universal scaling scheme (R-D model)

In phase 3, a simple analytic solution of the R-D equations yields [4,9]:

$$\Delta N_{IT} = [(k_F N_0) / k_R]^{1/2} (Dt)^n = S_N (Dt)^n \qquad (3)$$

By assuming identical E_A for k_F and k_R and a neutral H species, S_N and D become *only* dependent of E_{OX} and D respectively. This implies that ΔV_T (t) data measured at different E_{OX} (fixed T) and different T (fixed E_{OX}) can be respectively scaled by S_N (reaction term; only E_{OX} activated) and D (diffusion term; only T activated), as illustrated by Fig. 11. Also note that if the assumption of E_A (k_F) ~ E_A (k_R) is true, then (3) predicts that E_A (NBTI) ~ E_A (D)*n [7].

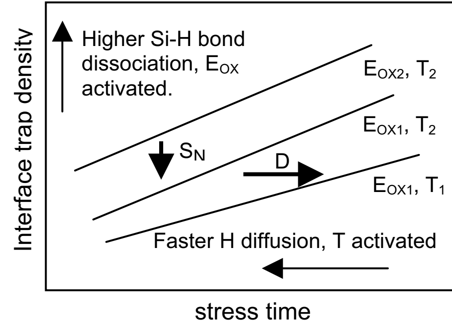

Fig. 11. Scaling scheme for ΔN_{IT} versus t data. Density axis reflects higher Si-H bond dissociation. Time axis denotes faster hydrogen diffusion. According to [4].

6. Experimental validation of R-D model

Fig.12 shows ΔN_{IT} for stress at various E_{OX} and T (low V_G, high T). ΔN_{IT} shows t^n (n~1/5) dependence at short time that increases at longer time. Break time (t_{BREAK}) decreases and the post-break slope (S_{BREAK}) increases with increase in T. However, t_{BREAK} and S_{BREAK} are insensitive to E_{OX}. This long-time ΔN_{IT} increase is unlike that observed at high V_G (section 2), and is a diffusion related process. Based on R-D model prediction, long-time ΔN_{IT} enhancement is due to absorption of H species into poly-Si (absorbing poly-Si) once the H diffusion front hits the SiO_2-poly-Si interface (at $t=t_{BREAK}$) [5]. As per Table-I, the time exponent n for $t < t_{BREAK}$ (phase-3, diffusion in oxide) suggests the H species as *neutral* H^O or H_2.

Moreover as per the universal scaling scheme (section 5), E_{OX} and T dependent data for $t < t_{BREAK}$ is scaled (see Fig. 12) along Y- and X-axis directions respectively to unique relations [4,7]. Y-axis scaling of varying E_{OX} data yields field activation of (total) NBTI, X-axis scaling of varying T data yields E_A of D, while Y-axis scaling of T dependent data (not shown) yields E_A of (total) NBTI.

Fig. 13 (top) plots the T activation of ΔN_{IT}, $1/t_{BREAK}$ and D. Obtained E_A (D) suggests H species as neutral H_2 [12]. E_A for NBTI (ΔN_{IT}) is related to E_A (D) by the time exponent n (~1/5), according to that predicted by the R-D model [7]. Furthermore, similar E_A for D and $1/t_{BREAK}$ confirms that the T activated enhanced ΔN_{IT} is a diffusion related phenomenon. As a proof, Fig. 13 (bottom) plots t_{BREAK} as a function of T_{PHY}. t_{BREAK} reduces with

T_{PHY} due to faster arrival of H_2 front into SiO_2-poly-Si interface for thinner T_{PHY}.

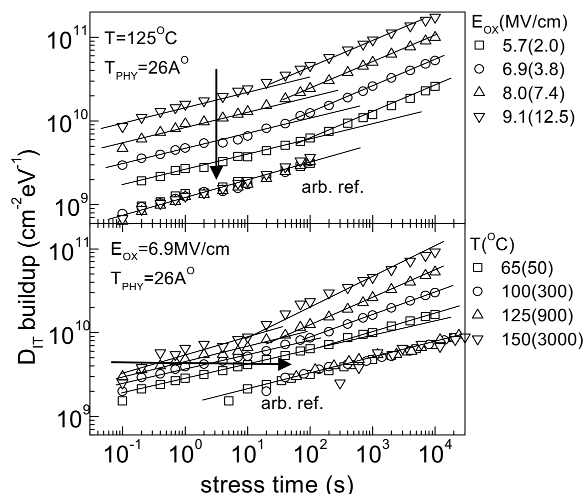

Fig. 12. Time evolution of ΔD_{IT} ($\sim\Delta N_{IT}$) for various stress E_{OX} and T (thermal, non-nitrided oxide). Pre-break E_{OX} and T dependent data is scaled by factors shown in brackets along Y- and X-axis respectively. Data from [7].

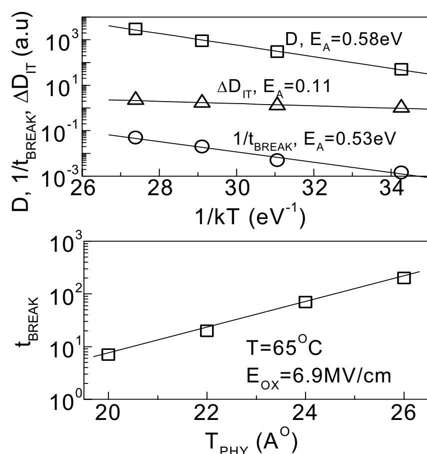

Fig. 13. (top) Temperature activation of $1/t_{BREAK}$, D (of H species in SiO_2) and ΔN_{IT} (NBTI activation). (bottom) t_{BREAK} as a function of T_{PHY}. Data from [7].

7. Recovery of interface traps

Fig. 14 shows the generation and recovery of ΔN_{IT} during and after NBTI stress. According to the R-D model, the forward reaction stops but the reverse reaction goes on once the stress is stopped. The H near the Si/SiO_2 interface rapidly anneals the broken Si- bonds, and creates a "diffusion hole". This drives further H diffusion (from the oxide bulk) towards the Si/SiO_2 interface and further recovery of ΔN_{IT} takes place [9]. Fig. 14 also shows that the R-D model can efficiently predict ΔN_{IT} buildup and recovery during both stress and post-stress phases. The H diffusion profile (for H^0) during recovery is shown in Fig. 15.

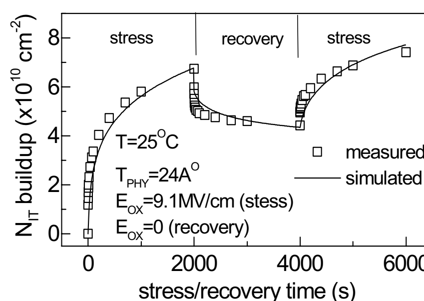

Fig. 14. Measured and simulated ΔN_{IT} for successive stress and recovery phases. Data from [7].

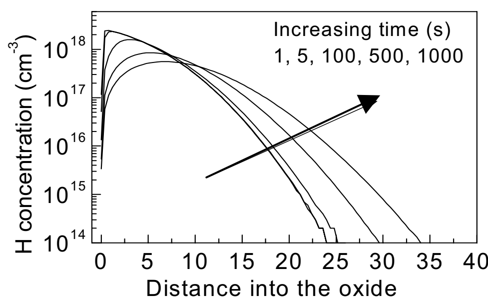

Fig. 15. H profile in the oxide during NBTI recovery, after 1000s stress. Parameters identical to Fig.10.

Identical ΔN_{IT} recovery is observed for successive stress-recovery cycles, while recovery is very weakly dependent on post-stress E_{OX} [6]. Of interest is ΔN_{IT} recovery measured at high T, especially after long-time stress in samples having absorbing poly-Si. Fig. 16 shows the magnitude of ΔN_{IT} generation and recovery and fractional recovery for 2000s stress and post-stress phases. The magnitude of ΔN_{IT} generation and recovery increases at larger T. However, the fractional recovery reduces at larger T (more ΔN_{IT} generation than recovery). This is due to H_2 loss or "lock-in" in poly-Si at higher T (due to faster D in poly-Si) [6], which results in less H_2 availability in the oxide for annealing the Si- bonds.

8. AC stress

Fig.17 shows the pulse frequency dependence of ΔN_{IT}. Degradation under AC is always lower than

that under DC NBTI [7,9,10]. ΔN_{IT} is frequency independent for lower f and the reduction (w.r.t DC) is due to recovery effects. At higher f, ΔN_{IT} reduces further due to non-equilibrium reaction effects, which can also be predicted from R-D simulations [9,10]. Significant lifetime improvement can be achieved for circuits under switching conditions.

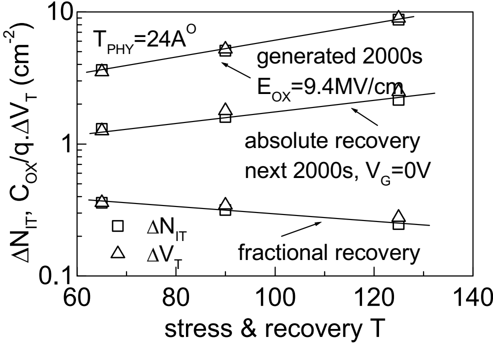

Fig. 16. Magnitude of ΔN_{IT} (and ΔV_T) generation and recovery and fractional ΔN_{IT} (and ΔV_T) recovery for 2000s stress and post-stress phases as a function of T (thermal, non-nitrided oxide).

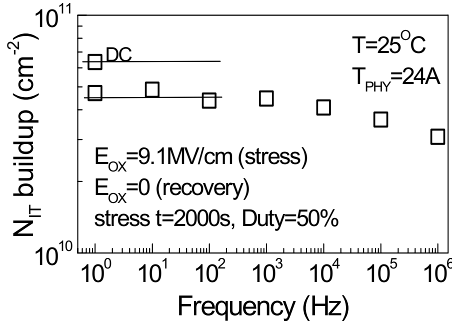

Fig. 17. Effect of pulse frequency on ΔN_{IT} buildup under AC stress. DC stress = 1000s, AC stress = 2000s with 50% duty cycle. Devices with thermal, non-nitrided oxides. Data from [7].

9. Effect of substrate bias

Fig. 18 (top) shows time evolution of ΔN_{IT} and ΔV_T for stress without and with reverse V_B. For V_B=0V stress $\Delta V_T \sim \Delta N_{IT}$ and shows a t^n power law with n~1/5. For V_B>0V stress, both ΔV_T and ΔN_{IT} increase at long time and show larger n. However, ΔV_T increases more than ΔN_{IT} for V_B>0V stress. It is important to note that similar to high V_G stress, SILC is observed for V_B>0V stress. Fig. 18 (bottom) shows V_B>0V stress induced enhanced (from V_B=0V stress) ΔV_T and ΔN_{IT}, together with ΔN_{OT} (C_{OX}/q. ΔV_T – ΔN_{IT}) and SILC as a function of stress time. All the quantities demonstrate a power-law time dependence with very similar time exponent (n ~ 0.5).

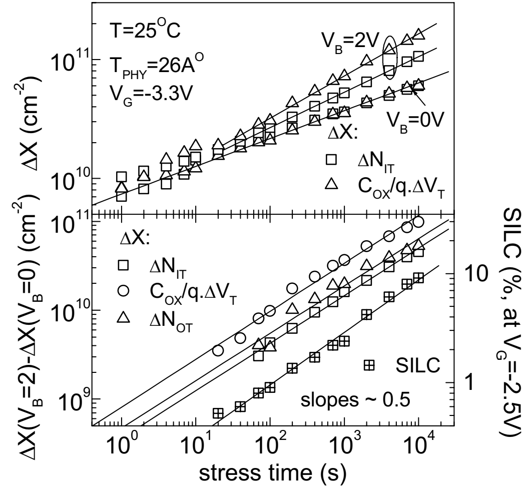

Fig. 18. (top) Time evolution of ΔV_T and ΔN_{IT} for V_B =0V and V_B>0V stress. (bottom) Enhanced ΔV_T, ΔN_{IT}, ΔN_{OT} and SILC as a function of stress time. Thermal, non-nitrided oxide. ΔX is ΔN_{IT}, ΔV_T or ΔN_{OT} (as explicitly mentioned in the legend).

Fig. 19 shows ΔN_{IT} generation (with and without V_B) and recovery for different post-stress bias. ΔN_{IT} recovery is weakly dependent on post-stress bias. It is important to note that the amount of ΔN_{IT} recovery is identical for stress with and without V_B, i.e., V_B>0V stress induced enhanced ΔN_{IT} does not recover.

Note, V_B>0V stress also causes impact ionization and HH generation [4]. HH creates ΔN_{OT}, which is due to broken Si-O bonds [11]. Mid-oxide broken Si-O bonds show up as SILC, while those near interface show up as additional ΔN_{IT}. Hence, additional ΔN_{IT} shows identical power-law exponent as SILC (see Fig. 18), and does not recover (see Fig. 19). Higher degradation due to V_B>0V stress is a serious concern and must be carefully addressed.

10. Effect of nitrogen

Fig.20 shows ΔV_T for different amount of N_2 content in the gate oxide. Data obtained from [13] for films grown by RTO and followed by RTN. ΔV_T always increases with increasing N_2 content (under identical stress condition), as also reported by others [14]. Though possible mechanism is yet unclear, it

has been suggested that N_2 reduces reaction energy [13] or creates hole-trapping centers [14], all of which can increase ΔV_T. N_2 induced enhanced NBTI is the primary concern for future technology nodes and needs urgent attention.

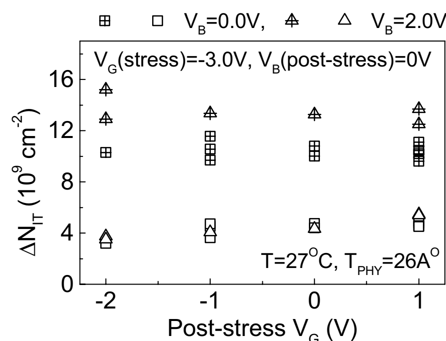

Fig. 19. ΔN_{IT} for 1000s stress (hashed symbol) with and without V_B and 1000s recovery (open symbol) for different post-stress bias (thermal, non-nitrided oxide).

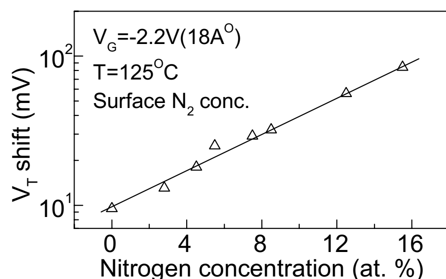

Fig. 20. ΔV_T for different nitrogen content in gate oxides. Data from [13].

11. Conclusions

The mechanism of NBTI is studied under a wide range of stress conditions. It is shown that high stress V_G must be avoided to minimize unwanted additional contribution from HH induced ΔN_{OT}. For "correct" stress, NBTI is purely due to ΔN_{IT} (in thermal, non-nitrided films) and is governed by inversion holes and E_{OX} (not by V_G and hot electrons). Generation and recovery of ΔN_{IT} is explained well with the R-D model, which shows that diffusion of H species plays an important role on time-rate of ΔN_{IT}. A universal data scaling methodology is presented, the diffusion species is identified as neutral H^0 or H_2, and relation between E_A of diffusion and E_A of overall NBTI is shown. It is shown that faster H^0 or H_2 diffusion in poly-Si increases the long-time degradation and reduces post-stress recovery. It is shown that ΔV_T is larger for V_B>0V stress because of additional contribution from ΔN_{OT}. Finally, NBTI is shown to increase for nitrided gate oxide, though the exact mechanism still unclear.

References

[1] D. Schroder and J. F. Babcock, Negative bias temperature instability: road to cross in deep sub-micron silicon semiconductor manufacturing, J. Appl. Phys., (94) 2003 1-18 (and references therein)

[2] K. Uwasawa, T. Yamamoto, and T. Mogami, A new degradation mode of scaled p+ polysilicon gate p-MOSFETs induced by bias temperature instability, in: Proc., IEDM, (1995) 871-874

[3] N. Kimizuka et. al., The impact of bias temperature instability for direct tunneling ultra-thin gate oxide on MOSFET scaling, in: Proc., VLSI Tech., (1999) 73-74

[4] S. Mahapatra and M. A. Alam, A predictive reliability model for PMOS bias temperature degradation, in: Proc., IEDM, (2002) 505-509

[5] S. Mahapatra, P. Bharath Kumar and M. A. Alam, A new observation of enhanced bias temperature instability in thin gate oxide p-MOSFETs, in: Proc., IEDM, (2003) 337-340

[6] S. Rangan N. Mielke and E. C. C. Yeh., Universal recovery behavior of negative bias temperature instability, in: Proc., IEDM, (2003) 341-344

[7] S. Mahapatra et. al., Mechanism of negative bias temperature instability in CMOS devices: degradation, recovery and impact of nitrogen", in: Proc., IEDM, (2004) 105-109

[8] K. O. Jeppson and C. M. Svensson, Negative bias stress of MOS devices at high electric fields and degradation of MOS devices, J. Appl. Phys., (48) 1977 2004-2014

[9] M. Alam, A critical examination of the mechanics of dynamic NBTI for p-MOSFETs, in: Proc., IEDM, (2003) 345-348

[10] S. Chakravarthi et. al., A comprehensive framework for predictive modeling of negative bias temperature instability, in: Proc., IRPS, (2004) 273-282

[11] J. D. Bude, B. E. Weir and P. Silverman, Explanation of stress induced damage in thin oxides, in: Proc., IEDM, (1988) 179-182

[12] M. L. Reed and J. D. Plummer, Chemistry of Si-SiO_2 interface trap annealing, J. Appl. Phys., (63), 1988 5776-5793

[13] S. S. Tan et. al., Neighboring effect in nitrogen-enhanced negative bias temperature instability, in: Proc., SSDM., (2003) 70-71

[14] V. Huard and M. Denais, Hole trapping effect on methodology for DC and AC negative bias temperature instability measurement in PMOS transistors, in proc., IRPS, (2004) 40-45